A three-dimension Dionne model for multipactor simulations

Adrien Plaçais, Mohamed Belhaj, Julien Hillairet, Jérôme Puech

A three-dimension Dionne model for multipactor simulations

A. Plaçais,[1] M. Belhaj,[2] J. Hillairet,[1] and J. Puech[3]
[1)] *CEA, IRFM, F-13108 Saint-Paul-Lez-Durance, France*
[2)] *DPHY, ONERA, Université de Toulouse F-31055 Toulouse, France*
[3)] *CNES, DSO/RF/HNO, F-31401 Toulouse, France*

(Dated: 6 February 2020)

The multipactor phenomenon is characterized by a very fast growth of the electronic population in Radio-Frequency (RF) devices under vacuum. As this effect limits the transmissible RF power and can harm RF systems, it has been widely studied during the last decades. Due to the high cost of experimental tests, simulation tools are heavily used to predict the threshold of multipactor growth. However, their reliability is limited for complex configurations, e.g. when dielectrics or magnetic fields are present. A crucial element of these multipactor simulations is the secondary-emission model. Dionne model is able to model both metals and dielectrics secondary emission but is one-dimension only. As the three-dimensional aspect is essential for complex configurations, the Dionne model is extended do three-dimensions. Measurements of the total electron emission yield have been carried out at the ONERA and shows a good agreement for low-impact energy and low-impact angle electrons, which is relevant in multipactor simulations.

I. INTRODUCTION

The multipactor effect is an electronic avalanche that may appear in vacuum RF systems when two conditions are met: (i) electrons enter in resonance with the RF field and (ii) their energy is sufficiently high to extract additional electrons from the system walls. In practice, multipactor appears when a RF electric field threshold $E_{\max}$ is reached. This phenomenon has been observed in telecommunications satellites[1] and in RF plasma heating systems of experimental fusion reactors (tokamaks)[2], but also in particle accelerators[3]. The multipactor creates an electron cloud, leading to a disturbance or even a reflection to the source of RF signal. A breakdown can also be created, leading to a rapid heating of the surfaces, an alteration of the system material's properties or an out-gassing triggering the destructive corona effect[4].

As multipactor threshold measurements are expensive, alternative methods have been developed to estimate it: theoretical[5,6] and statistical[7] studies, Monte-Carlo[8] or Particle-in-Cell (PIC) simulations[9,10]. A PIC code has been developed in[11,12] in order to understand the apparition of this phenomenon in complex RF devices from a physical point of view. This approach requires an accurate modelling of the physics at stake, and especially of the electron emission phenomenon.

Let us consider a sample impacted by a flux of electrons, called Primary Electrons (PEs). A second flux of electrons may be emitted by the sample; it is made up of Secondary Electrons (SEs, which are electrons removed from the material), of Inelastically and Elastically Backscattered Electrons (IBEs and EBEs, which are PEs rediffused by the sample respectively with and without energy loss). The Secondary Electron Emission Yield (δ, SEEY) is defined as the ratio between the SEs and PEs fluxes. It is higher than one if there are more SEs than PEs. The Elastically Backscattered Electron Emission Yield (η_e, EBEEY) and Inelastically Backscattered Electron Emission Yield (η_i, IBEEY) are similarly defined. Finally, the Total Electron Emission Yield (σ, TEEY) is the ratio between all emitted electrons and PEs fluxes. $\sigma > 1$ is a necessary condition for the electron population to grow and thus for the multipactor to appear. We have the relation:

$$\sigma = \delta + \eta_e + \eta_i \tag{1}$$

A full modelling of the three emitted electrons populations require the knowledge of their emission yields, as well as their energies and angular distributions. All these quantities rely on the energy and direction of the PEs flux[13], on the surface morphology of the sample[14], on the presence of contaminants[15] or external magnetic fields[16]. In addition, dielectric materials, which are widely used in spacecraft applications, can hold a net electric charge. It influences electron emission through two processes: firstly, the created surface potential may have an effect on electrons trajectories in the vacuum. Secondly, the excess of holes or electrons inside the material modifies the transport of electrons when they are in the sample. SEs are the population the most influenced as they are the least energetic.

As SEs are the predominant population in waveguides, the SEEY mostly conditions the multipactor apparition. SEEY models exist[17–19], but, to our knowledge, Dionne model[20] is the only one able to take into account the influence of dielectrics charge on the transport of SEs inside the material[21] while being sufficiently simple for PIC simulations, which involve large numerical resources. Another asset of Dionne is that it gives δ, while some other models only give σ[22–24]. Thus, Dionne model allows SEs to be discriminated from backscattered electrons. EBEs have been shown to be of great importance in multipactor apparition[25], especially when magnetic fields are present[26]. EBEs were also shown to be significant in Hall plasma thrusters energy balance[27].

The main limitation of Dionne model is that it is one-dimension only and cannot take into account for the incidence angle of PEs; this restriction becomes a limitation

when simulating complex 3D geometries such as circulators. Circulators are used to avoid RF power reflection to the source, that would cause it's degradation. The central part of circulators is composed of ferrites that may have a dielectric behavior; they also create a static magnetic field parallel to the RF electric field, reason why a three-dimension simulation becomes mandatory.

In this paper, we develop a three-dimension version of Dionne model for such configurations. In section II, we make a simple simulation to evaluate the validity range relatable for multipactor study. In section III, we develop the secondary emission model. Finally, we benchmark it with in-house electron emission yield measurements in section IV.

II. MODEL FRAMEWORK

We define here the validity range of the proposed SEEY model in terms of PEs impact energy and incidence angle. Preliminary multipactor simulations have been made with the simulation code POTOMAC (Physical simulatiOn TOol for Multipactor in Advanced Configurations)[11,12]. POTOMAC is a PIC code that computes the evolution of the electron population in a domain with a given RF electric field. Each time a collision occur, δ, η_e and η_i are calculated and the appropriate emission mechanism is chosen. Here, the multipactor threshold was computed for a WR75 rectangular waveguide with silver coated walls. This basic configuration was chosen for the sake of simplicity; we saw that adding magnetic fields or dielectrics did not change the order of magnitude of PEs impact energy and incidence angle. The RF signal has a frequency of 11 GHz and propagates in the $TE_{1,0}$ mode, which is the fundamental mode for this geometry. Dimensions are $19.05\,\text{mm} \times 9.525\,\text{mm}$. The used electron emission models are listed in Tab. I.

	Emission Yield	Angular distrib.	Energy distrib.
SE	Dionne (this paper)	Cosine law[28]	Chung *et al.*[29]
EBE	SLAB[30]	SLAB[30]	Monoenergetic
IBE	Constant	Cosine law[28]	Uniform

TABLE I: Full electron emission model used with POTOMAC for the preliminary simulation

We recorded the impact energy of all PEs at the multipactor threshold and represented it as an histogram in Fig. 1. These results first show that SEs are predominant in POTOMAC simulations, and thus must be modelled with great attention. Secondly, 99 % of PEs impact the walls with an energy lower than 230 eV. In order to take into account for the various configurations, the model should be valid up to 300 eV.

Fig. 2 is an histogram of the SEs angular flux when they impact a wall, θ_0 being defined prior to the wall normal (see Fig. 3). It shows us that the majority of SEs impact surfaces almost perpendicularly; as we want our model to be usable in the broadest variety of scenarios possible, it should be valid for angles ranging from 0° to 40°.

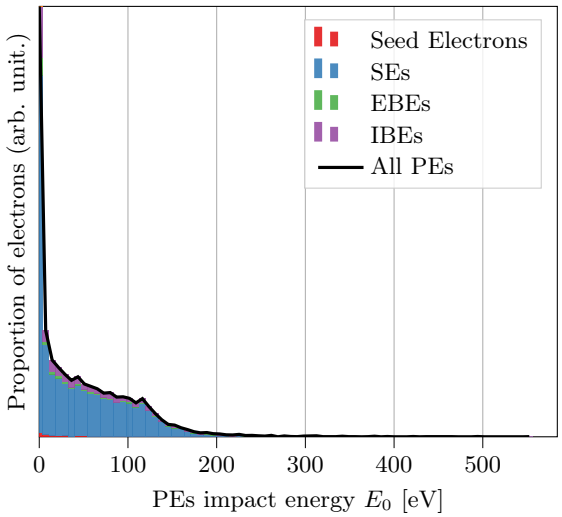

FIG. 1: Histogram of the PEs impact energy

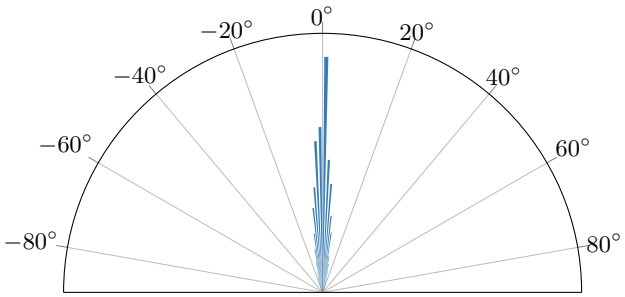

FIG. 2: Histogram of the SEs impact angle θ_0

The model we propose can be used in other fields than multipactor, as long as electrons impact surfaces with a low energy and a low incidence angle.

III. SEEY MODEL

A. Dionne in 1D

Numerous secondary emission models already exist; for example, Monte-Carlo methods are precise and can take into account all the physical processes involved, but are very slow, which is prohibitive for PIC simulations. On the other side of the spectrum, very fast and simple models exist, such as Vaughan[22,23]. This model is 3D and can take into account the materials rugosity. However, it has the inconvenient of returning a null TEEY for very low energy PEs, which constitutes an important proportion of impacting electrons (see Fig. 1) and is not consistent

with measurements[31]. Plus, this model cannot discriminate SEs from IBEs and EBEs. A modified version of Vaughan has been proposed[32], which manually forces a TEEY equal to unity for low-energy electrons; it also fits a parameter $E_{\text{threshold}}$ to enforce the model to match the first cross-over point, which has been shown of being of primordial importance for multipactor simulations[33]. The modified Vaughan model is widely used by the multipactor community.

Dionne model is a fast, simple and physical model for the SEEY. It makes the assumption that secondary emission process can be divided into three steps:

1. a PE enter a sample and emit SEs on its trajectory inside the material;
2. SEs are transported from their emission point to the surface;
3. SEs escape the sample through the surface.

All terms in Dionne model have a physical meaning. Thus, it is for example possible to analytically reflect the influence thin coatings have on the SEEY and hence on the multipactor[12,34]. However, Dionne model does not take into account for the incidence angle of the PE, unlike Vaughan.

For the sake of clarity, Dionne model is explained here. Under the hypothesis of a constant energy loss for the PE and no scattering for the SEs, it may be written as:

$$\delta = G \cdot T \cdot S \tag{2}$$

Where the generation term G represents the mean number of SEs produced by the PE, the transmission term T represents the probability for the produced SEs to reach the surface and the escape term S is a sample dependent constant representing the probability for the SEs to cross the surface. This terms can be expressed as:

$$G = \frac{E_0^n}{\Phi \cdot R(E_0)} \tag{3}$$

$$T = d \cdot \left(1 - \mathrm{e}^{-R(E_0)/d}\right) \tag{4}$$

Where n is a material dependent constant, E_0 is the energy of the PE and Φ the material effective work function[35] defined prior to the vacuum level in eV. For a metal, $\Phi = W_f$ with W_f the work function and for a dielectric, $\Phi = \chi + E_g$ with χ the electron affinity and E_g the gap energy. R is the range of the PE (see Fig. 3) and d the diffusion length of the PE in the material in nm. Using the continuous slowing down approximation, with A a surface-dependent constant, the range can be expressed as[20,36]:

$$R(E_0) = \frac{E_0^n}{A \cdot n} \tag{5}$$

Φ can be measured or calculated[37]. d can be linked with the inelastic mean-free path[38]; however, very low energy electrons trajectories are mostly driven by elastic collisions[17], making this assumption unsuitable for our study. d also can be calculated with the density and the effective absorption coefficient[39]. Thermionic emission experiments allow us to measure S[39]. A and n can be extracted from Monte-Carlo simulations or measurements[36].

In this study, Φ will be taken from literature while A, n, d and S will be fitted, for that they drastically vary from one sample to another – especially when samples are contaminated.

B. Dionne in 3D

At a given energy and if the considered sample is perfectly flat, PEs penetrate less and less deep while θ_0 increases (see Fig. 3). Thus, SEs are emitted closer and closer to the surface and are more likely to be emitted in the vacuum, increasing the SEEY.

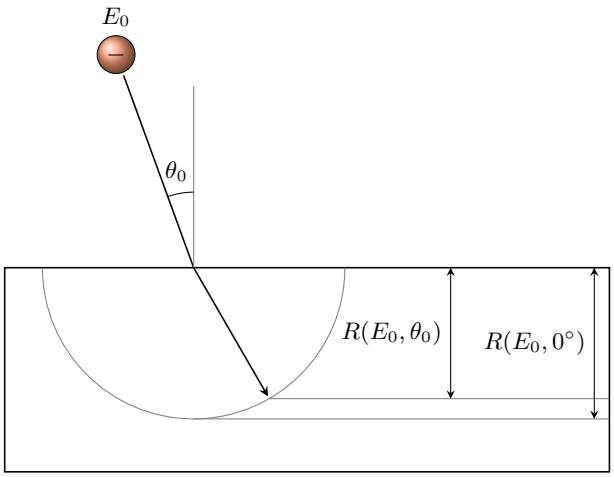

FIG. 3: Macroscopic view of a PE impacting a sample with an energy E_0 and an angle θ_0

Dionne model was not designed to take the incidence angle θ_0 into account. As it is physical, it is however possible to add an angle dependency. Modifying θ_0 does not influence the distance travelled by the PE but only its range (see Fig. 3). The Snell's law for electron reads[40]:

$$\sqrt{E_0}\sin\theta_0 = \sqrt{E_1}\sin\theta_1 \tag{6}$$

where E_1 and θ_1 are respectively the energy and angle of the electron after it has been refracted in the sample. The range thus can be expressed as:

$$R(E_0, \theta_0) = R(E_0, 0°)\sqrt{1 - \frac{E_0}{E_0 + \Phi} \cdot \sin^2\theta_{\text{equ}}} \tag{7}$$

With θ_{equ} the equivalent incidence angle. This notion was first used to take into account the fact that the macroscopic angle θ_0 is different from the real impact

angle for a non perfectly flat sample (oblique incidence effect), due to the surface roughness. Other phenomenons are to be taken into account: if the sample presents a small roughness, low-energy high incidence angle electrons that could not be emitted on a flat surface can escape an inclined plane, increasing the SEEY at low energy[14]. For high roughness materials, SEs are more likely to be recollected by the sample, which causes a reduction of the SEEY (shading effect)[14]. This effect is more pronounced in presence of magnetic fields[16]. Recollected SEs can also emit other electrons (multigeneration).

Zhang *et al.*[41] showed with Monte-Carlo simulations that it was possible to replace θ_0 with θ_{equ} in TEEY calculations to take all these effects into account, for random rough surfaces with Gaussian height distribution. Their results suggested that a first order approximation could be:

$$\theta_{\text{equ}}(\theta_0) = k_a\theta_0 + k_b \tag{8}$$

With k_a and k_b rugosity profile dependent constants. For a perfectly flat material, $\theta_{\text{equ}} = \theta_0$ which implies $k_a = 1$ and $k_b = 0°$.

IV. MODEL VERIFICATION

A. Experimental procedure

The TEEY measurements were performed in Ultra High Vacuum (UHV) facility designed to the study of electron emission. A dry turbo-molecular pump associated with an oil-free primary pump allows the system to be maintained at a vacuum level down to 3×10^{-9} mbar. The sample holder allows the variation of the electron incidence angle from 0° (normal incidence angle) to 80°. An ELG-2022B electron gun from Kimball Instrument was used. The electron beam was pulsed during TEEY measurements to limit the surface conditioning effect[42]. The facility is equipped with a Faraday cup, a hemispherical electron energy analyser and a X-ray Mgkalpha source. The sample holder and the collector can be independently biased to choose the desired potential. The sample holder is ordinarily negatively biased in order to prevent the low energy emitted electron to come back to the sample surface and prevent the generation of tertiary electrons.

TEEY measurements were made on several samples (associated dataset available at `http://dx.doi.org/10.5281/zenodo.3648704`[43]). The first sample, called hereafter Cu #1, was heated *in situ* and under UHV at 200 °C for 2 h. A second set of measurements was made after 3 h of *in situ* erosion under 1 keV Ar^+ flux at normal incidence. XPS study showed that after the heating, the sample was contaminated, mainly with oxygen and carbon; after the erosion, it was almost pure.

A second set of measurements was made on another copper sample, Cu #2. Measurements were made on the sample without any treatment (as received), after 2 h of heating at 200 °C *in situ* and under UHV, and after 1 h of *in situ* erosion under 1 keV Ar^+ flux at normal incidence.

B. Fitting process

The total backscattered electron emission yield η is defined as:

$$\eta = \eta_e + \eta_i \tag{9}$$

We computed η with the Monte-Carlo software CASINO v3.3.0.4[44]. ELSEPA model was used for the total and partial cross-section calculation[45], the directing cosin was calculated with Lowney *et al.*[46], the stopping power and ionisation potential with Joy *et al.*[47]. The pseudo-random number generator was a Lagged Fibonacci generator. Results showed a very weak dependence of η on θ_0.

We computed η_e with SLAB model[30]. Due to the lack of literature on the subject, we considered that η_i was a constant, independent from E_0 and θ_0. As our values of η and η_e are accurate for $E_0 = 500$ eV and $\theta_0 = 0°$, we set η_i so that Eq. (9) holds at 500 eV and 0°. Dionne model was then fitted on measurements with E_0 in 0–300 eV and θ_0 in 0°–40° .

Dionne model was compared to modified Vaughan model as defined in[32]. For almost all materials, Vaughan rugosity parameters k_E and k_θ should be equal to unity. They may be lower for intentionally roughened materials, down to 0 for textured carbon. They may be up to 2 for extremely smooth surfaces. Modified Vaughan parameter $E_{\text{threshold}}$ and Vaughan rugosity parameters were also fitted on 0–300 eV and 0°–40° , k_E and k_θ being constrained between 0.5 and 2.

C. Sample Cu #1 results

The measured and fitted TEEY for the sample Cu #1 after heating are represented Fig. 4. Results show an overall good agreement between the proposed model and measurements, on the validity range we defined. TEEY is slightly underestimated for very low energies, the error increasing with θ_0. $\sigma(E_0, 60°)$ is wildly overestimated. Vaughan model does not correctly reproduce the shape of the curves, but is closer to measures than Dionne for $\theta_0 = 60°$.

The results for eroded Cu #1 are represented Fig. 5. Here, the general shape of the TEEY is reproduced on the chosen validity range. However, it cannot reproduce the fact that $\sigma(E_0, 0°) > \sigma(E_0, 20°)$. Plus, the TEEY drastically increases at 60° and is thus underestimated by the model. Vaughan results are similar to Dionne.

The obtained fitting parameters for Cu #1 are summarized in Tab. II.

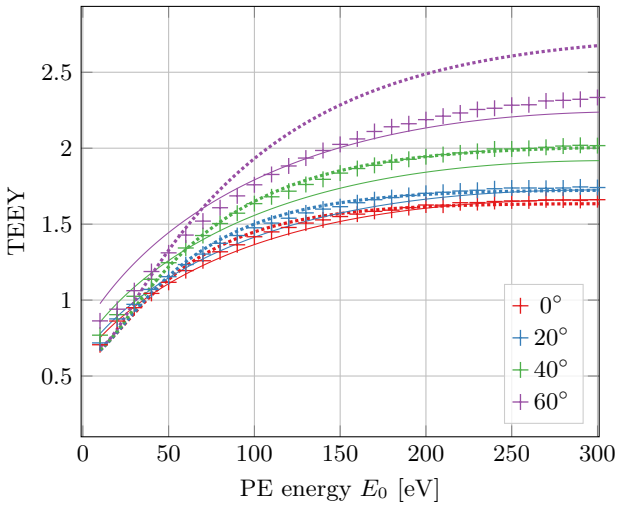

FIG. 4: Measured and fitted TEEY on Cu #1 (heated; + measures, ····· Dionne fit, —— Vaughan fit). [Associated dataset available at `http://dx.doi.org/10.5281/zenodo.3648704`[43]]

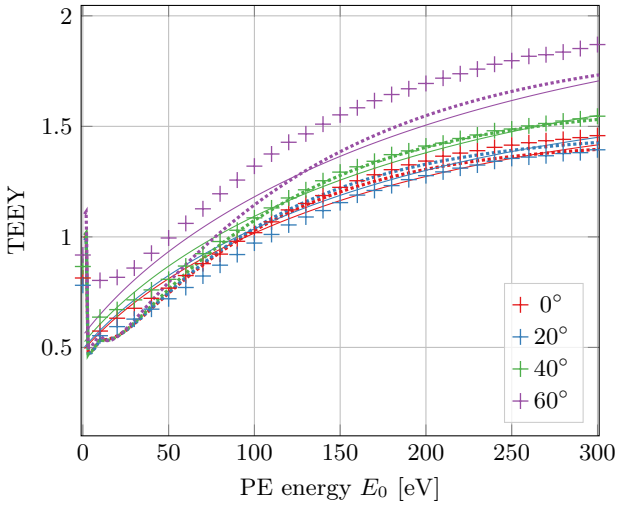

FIG. 5: Measured and fitted TEEY on Cu #1 (eroded; + measures, ····· Dionne fit, —— Vaughan fit). [Associated dataset available at `http://dx.doi.org/10.5281/zenodo.3648704`[43]]

D. Sample Cu #2 results

The results for the sample Cu #2 without any surface treatment are represented Fig. 6. Both Dionne and Vaughan fits work very well on the whole energy and angle ranges, and Dionne even fits 60° which is out of the validity range.

Heated Cu #2 results are represented in Fig. 7. For $\theta_0 \in [0°, 40°]$, Dionne model is in accordance with data. For $\theta_0 = 60°$, however, the TEEY is overestimated; the measured TEEY is higher at 60° than at 40°, which cannot be reproduced by Eq. (8). For the first measure point at 10 eV, the TEEY varies sharply with θ_0. Vaughan model underestimates the TEEY.

Finally, the measured and fitted TEEY of eroded Cu #2 are represented Fig. 8. For $\theta_0 \leq 20°$, Dionne fit is rather good and matches the measures. However, it underestimates σ for $\theta_0 = 40°$. The measured TEEY at 60° is lower than the TEEY at 40°, leading to a wide overestimation of the measures. Vaughan results are very similar to Dionne for 0° to 40°.

All fitting parameters are listed in Tab. III.

	Heated	Eroded
A	7.75	8.30
n	1.00	1.00
d [nm]	6.23	11.40
S	0.13	0.06
k_a	0.92	0.74
k_b [°]	2.26	0.00
Φ [eV]	4.65	–
η_i	0.25	–
Vaughan $\sigma_{\max}$	1.66	1.53
Vaughan $E_{\max}$ [eV]	300	550
Vaughan $E_{\text{threshold}}$ [eV]	−21.82	−28.93
Vaughan k_E	0.50	1.37
Vaughan k_θ	2.00	1.56

TABLE II: Evolution of Cu #1 fitting parameters

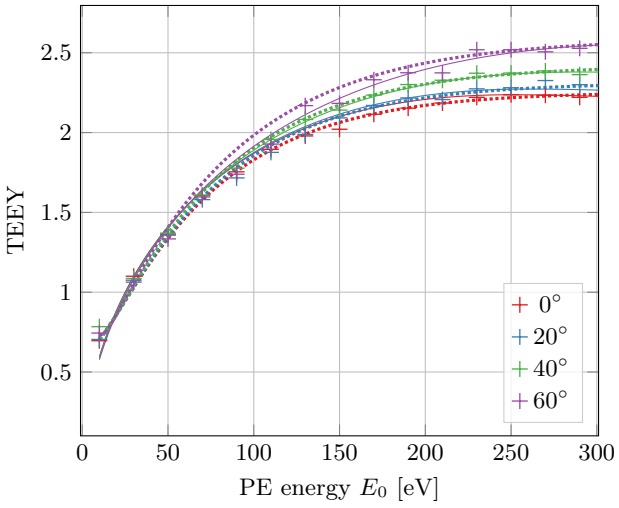

FIG. 6: Measured and fitted TEEY on Cu #2 (as received; + measures, ····· Dionne fit, —— Vaughan fit). [Associated dataset available at `http://dx.doi.org/10.5281/zenodo.3648704`[43]]

V. DISCUSSION

The proposed model works very well on the defined validity range (i.e. , E_0 in 0–300 eV and θ_0 in 0°–40°).

Results however show some discrepancy in the very

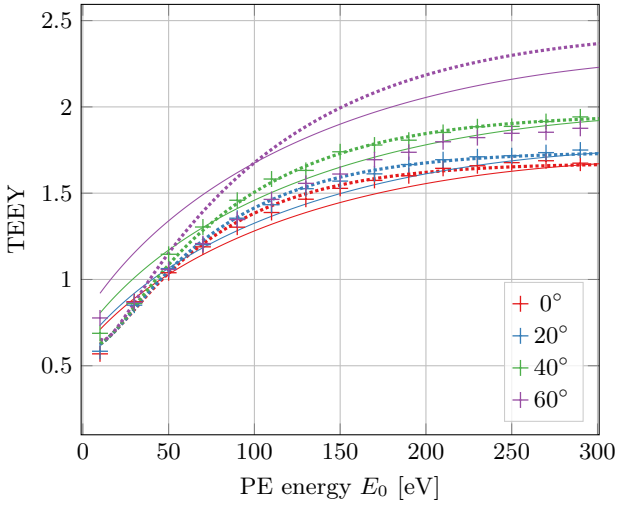

FIG. 7: Measured and fitted TEEY on Cu #2 (heated; + measures, ····· Dionne fit, —— Vaughan fit). [Associated dataset available at `http://dx.doi.org/10.5281/zenodo.3648704`[43]]

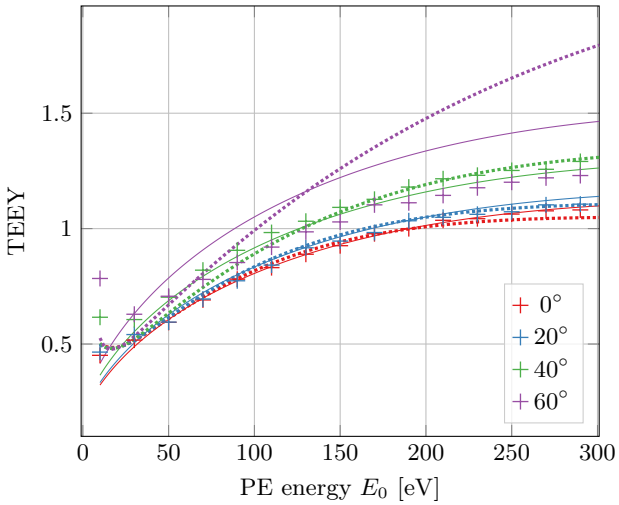

FIG. 8: Measured and fitted TEEY on Cu #2 (eroded; + measures, ····· Dionne fit, —— Vaughan fit). [Associated dataset available at `http://dx.doi.org/10.5281/zenodo.3648704`[43]]

low energy range ($\lessapprox$ 20 eV), especially for non-normal incidences and eroded materials. We propose several explanations; firstly, the range expression (Eq. (5)) was obtained with the hypothesis that electrons lost their energy in the material in a continuous way (continuous slowing down approximation), which is inexact at low energies. In reality, the range may be constant below a few tenths of eV[48,49]. Secondly, we set a constant IBEEY as we lack literature on the subject, which is a very strong hypothesis.

In Fig. 9, we represented θ_{equ} as a function of θ (Eq. (8)) for the different materials, with the values of k_a and k_b listed in Tab. II and III. We also represented Zhang *et al.* results, obtained with Monte-Carlo simulations; the three black lines represent the evolution of the equivalent angle for three copper samples with different random rugosity profiles[41]. As we can see, the linear approximation for the θ_{equ} law is justified. However, the materials studied in this paper all seem to be softer than Zhang's.

	As received	Heated	Eroded
A	5.21	5.03	8.73
n	1.00	1.00	1.11
d [nm]	9.71	12.28	18.76
S	0.14	0.10	0.04
k_a	0.14	0.83	1.18
k_b [°]	37.19	1.12	0.00
Φ [eV]	4.65	–	–
η_i	0.25	–	–
Vaughan $\sigma_{\max}$	2.24	1.70	1.12
Vaughan $E_{\max}$ [eV]	250	390	390
Vaughan $E_{\text{threshold}}$ [eV]	1.11	−25.09	−6.51
Vaughan k_E	2.00	0.50	0.50
Vaughan k_θ	0.82	2.00	2.00

TABLE III: Evolution of Cu #2 fitting parameters

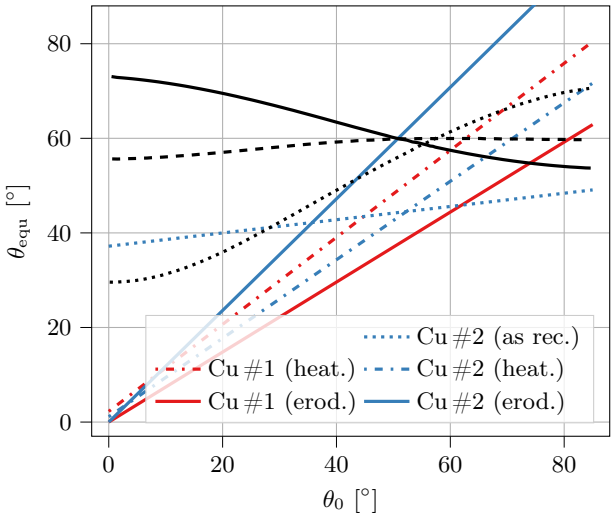

FIG. 9: θ_{equ} laws for different materials; black lines represent Zhang *et al.* simulation results on different random surfaces with a Gaussian height profile[41]

All trends are not faithfully reproduced when increasing θ_0 leads to a reduction of σ (i.e. Cu #1 eroded, Cu #2 heated, Cu #2 eroded). In these cases, the variation of σ with θ_0 is non monotonous, which cannot be reproduced by Eq. (8). Using higher-order polynomials for the relation between θ_0 and θ_{equ} does solve the issue, but this approach is inconsistent with available literature[41]. New emission yield measurements campaigns associated with rugosity profile studies would be required to investigate further the relation between θ_0 and θ_{equ}. Also, the

hypothesis of a random rough surface with a Gaussian height distribution may be not representative of the real surface profile.

For the two materials, the surface treatments reduce contamination and thus the emission yield. As SEs have a low energy, the only one able to escape are produced in the first nanometers below the surface. Thus, they are very influenced by the presence of contaminants[15]. For both samples, the reduction of the contamination layer reduces the parameter k_b, which is 0 for eroded coppers. Our interpretation is that, for this materials, the contamination layer at the surface of the samples has a rougher surface state than the bulk material underneath; this is particularly noticeable on Cu #2, where the difference of rugosity between the sample without any surface treatment and after the heating is tremendous. It is to be noted that, even for clean materials with $k_a \approx 1$ and $k_b \approx 0$, the introduction of θ_{equ} increased the accuracy of our model.

Here, Dionne model was shown to be more precise than modified Vaughan model at low energy. It is to be noted that Vaughan fit was much better than Dionne for energies higher than a few hundreds of eV, and that it's implementation is easier. Vaughan rugosity parameters are often inconsistent, for example for heated Cu #2, where $k_E = 0.50$ suggests that the sample is very rough, while $k_\theta = 2.00$ tells the exact opposite. Plus, Vaughan always underestimates the TEEY at 10 eV.

VI. CONCLUSIONS

In this paper, we developed a simple extension of Dionne model to three-dimension. We used the refraction law for electrons to compute the range of electrons for various incidence angles. We used the concept of equivalent angle θ_{equ} to model the differences between macroscopic and microscopic incidence angle, as well as shading and multigeneration effects.

The present model was compared to in-house measurements on two copper samples with several surface treatments. The fit was made on the low-energy range (0–300 eV) and low-angle range (0–40°), which is relevant for multipactor simulations. As a whole, the model fit experimental data in these ranges. The fit is however less good for high incidence angles and low energies, as well as for some materials where the evolution of σ with θ_0 is not monotonous. Fits on silver led to similar results but were not included in this publication.

The introduction of θ_{equ} was indispensable for the most contaminated material (Cu #2 as received), but also greatly increased the accuracy of the fit for purer materials. The relation between θ_0 and θ_{equ} should be explored, with Monte-Carlo simulations and emission yield measurements associated with rugosity profile studies. As magnetic fields were shown to influence electron emission from rough samples[16], studying the link between θ_{equ} and magnetic fields would be another step towards extensive multipactor studies in presence of magnetic fields.

A comparison was made with modified Vaughan model, widely used in the multipactor community. At very low energy, Dionne model showed to be more precise. At higher energies up to 300 eV, Dionne model gave similar or better results than Vaughan.

Several points could enhance the model: firstly, it has been proved that SLAB model was too simplistic[50] and thus could be replaced by OKGM model even if it generally underestimates η_e[51,52]. Secondly, the modeling of η_i is also simplistic – we lack a simple physical model for the IBEEY. Finally, the used range function is not valid on the whole energy range, R being almost constant below a few tenths of eV[48,49].

ACKNOWLEDGMENTS

This work has been carried out within the framework of the EUROfusion Consortium and has received funding from the Euratom research and training programme 2014-2018 and 2019-2020 under grant agreement No 633053. The views and opinions expressed herein do not necessarily reflect those of the European Commission.

[1] J. de Lara, F. Perez, M. Alfonseca, L. Galan, I. Montero, E. Roman, and D. Garcia-Baquero, "Multipactor prediction for on-board spacecraft RF equipment with the MEST software tool," IEEE Transactions on Plasma Science **34**, 476–484 (2006).

[2] M. Goniche, C. El Mhari, M. Francisquez, S. Anza Hormigo, J. Belo, P. Hertout, and J. Hillairet, "Modelling of power limit in RF antenna waveguides operated in the lower hybrid range of frequency," Nuclear Fusion **54**, 013003 (2014).

[3] C. Bourat and J.-M. Joly, "On multipactor effect in a 600 MHz RF cavity used in electron linear accelerator," IEEE Transactions on Electrical Insulation **24**, 1045–1048 (1989).

[4] E. Sorolla, *Contribution to modeling multipactor and corona discharges in high power electromagnetic fields*, Ph.D. thesis, École Polytechnique Fédérale de Lausanne (2012).

[5] A. J. Hatch and H. B. Williams, "Multipacting Modes of High-Frequency Gaseous Breakdown," Physical Review **112**, 681–685 (1958).

[6] E. F. Vance, "One-Sided Multipactor Discharge Modes," Journal of Applied Physics **34**, 3237–3242 (1963).

[7] A. G. Sazontov, V. A. Sazontov, and N. K. Vdovicheva, "Multipactor Breakdown Prediction in a Rectangular Waveguide: Statistical Theory and Simulation Results," Contributions to Plasma Physics **48**, 331–346 (2008).

[8] V. E. Semenov, E. I. Rakova, D. Anderson, M. Lisak, and J. Puech, "Multipactor in rectangular waveguides," Physics of Plasmas **14**, 033501 (2007).

[9] M. Francisquez, *Power Limit Modeling of Lower Hybrid Antenna Waveguides in Tokamaks*, Bachelor of arts honors thesis, Dartmouth College (Hanover, NH) (2012).

[10] C. Chang, G. Liu, C. Tang, C. Chen, and J. Fang, "Review of recent theories and experiments for improving high-power microwave window breakdown thresholds," Physics of Plasmas **18** (2011), 10.1063/1.3560599.

[11] E. Sorolla, M. Belhaj, J. Sombrin, and J. Puech, "New multipactor dynamics in presence of dielectrics," Physics of Plasmas **24**, 103508 (2017).

[12] A. Plaçais, E. Sorolla, M. Belhaj, J. Hillairet, and J. Puech, "Influence of work function on the multipactor threshold," in *2018 IEEE MTT-S International Conference on Numerical Electromagnetic and Multiphysics Modeling and Optimization (NEMO)* (IEEE, Reykjavik, Iceland, 2018) pp. 1–4.

[13]A. Dekker, "Secondary Electron Emission," in *Solid State Physics*, Vol. Volume 6 (1958) pp. 251–311.

[14]K. Nishimura, T. Itotani, and K. Ohya, "Influence of Surface Roughness on Secondary Electron Emission and Electron Backscattering from Metal Surface," Japanese Journal of Applied Physics **33**, 4727–4734 (1994).

[15]T. Gineste, M. Belhaj, G. Teyssedre, and J. Puech, "Investigation of the electron emission properties of silver: From exposed to ambient atmosphere Ag surface to ion-cleaned Ag surface," Applied Surface Science **359**, 398–404 (2015).

[16]N. Fil, M. Belhaj, J. Hillairet, J. Puech, and R. Mathevet, "Electron emission under uniform magnetic field of materials for fusion and space applications," Fusion Engineering and Design (2017), 10.1016/j.fusengdes.2017.03.039.

[17]M. A. Furman and M. T. F. Pivi, "Probabilistic model for the simulation of secondary electron emission," Physical Review Special Topics - Accelerators and Beams **5**, 124404 (2002).

[18]M. A. Furman and M. T. F. Pivi, "Erratum: Probabilistic model for the simulation of secondary electron emission [Phys. Rev. ST Accel. Beams 5 , 124404 (2002)]," Physical Review Special Topics - Accelerators and Beams **16**, 069901 (2013).

[19]D. Sydorenko, *Particle-in-Cell Simulations of Electron Dynamics in Low Pressure Discharges with Magnetic Fields*, Ph.D. thesis, University of Saskatchewan, Canada (2006).

[20]G. F. Dionne, "Effects of secondary electron scattering on secondary emission yield curves," Journal of Applied Physics **44**, 5361–5364 (1973).

[21]N. Balcon, M. Belhaj, T. Tondu, J. C. Mateo-Velez, and D. Payan, "Secondary electron emission of cover glasses: Temperature and incident flux effects," in *International Symposium on Materials in the Space Environment*, edited by L. Ouwehand (ESA Communications, Noordwijk, The Netherlands, 2013).

[22]J. Vaughan, "A new formula for secondary emission yield," IEEE Transactions on Electron Devices **36**, 1963–1967 (1989).

[23]J. Vaughan, "Secondary emission formulas," IEEE Transactions on Electron Devices **40**, 830 (1993).

[24]S. Barral, K. Makowski, Z. Peradzyński, N. Gascon, and M. Dudeck, "Wall material effects in stationary plasma thrusters. II. Near-wall and in-wall conductivity," Physics of Plasmas **10**, 4137–4152 (2003).

[25]R. Seviour, "The Role of Elastic and Inelastic Electron Reflection in Multipactor Discharges," IEEE Transactions on Electron Devices **52**, 1927–1930 (2005).

[26]M. S. Feldman, A. A. Hubble, R. Spektor, and P. T. Partridge, "Effects of Backscattered Electrons on Multipactor Simulations with Parallel Magnetic Fields," in *2018 IEEE MTT-S International Conference on Numerical Electromagnetic and Multiphysics Modeling and Optimization (NEMO)* (IEEE, Reykjavik, Iceland, 2018) pp. 1–3.

[27]M. Villemant, P. Sarrailh, M. Belhaj, C. Inguimbert, and L. Garrigues, "Modélisation de l'émission secondaire dans les propulseurs à courant de Hall et les applications RF," Tech. Rep. (ONERA, Toulouse, France, 2017).

[28]J. Greenwood, "The correct and incorrect generation of a cosine distribution of scattered particles for Monte-Carlo modelling of vacuum systems," Vacuum **67**, 217–222 (2002).

[29]M. S. Chung and T. E. Everhart, "Simple calculation of energy distribution of low-energy secondary electrons emitted from metals under electron bombardment," Journal of Applied Physics **45**, 707–709 (1974).

[30]A. Jablonski, P. Mrozek, G. Gergely, M. Menhyárd, and A. Sulyok, "The inelastic mean free path of electrons in some semiconductor compounds and metals," Surface and Interface Analysis **6**, 291–294 (1984).

[31]R. Cimino, L. A. Gonzalez, R. Larciprete, A. Di Gaspare, G. Iadarola, and G. Rumolo, "Detailed investigation of the low energy secondary electron yield of technical Cu and its relevance for the LHC," Physical Review Special Topics - Accelerators and Beams **18**, 051002 (2015).

[32]C. P. Vicente, M. Mattes, D. Wolk, B. Mottet, H. Hartnagel, J. Mosig, and D. Raboso, "Multipactor breakdown prediction in rectangular waveguide based components," in *IEEE MTT-S International Microwave Symposium Digest, 2005.*, Vol. 2005 (IEEE, 2005) pp. 1055–1058.

[33]N. Fil, M. Belhaj, J. Hillairet, and J. Puech, "Multipactor threshold sensitivity to Total Electron Emission Yield in parallel-plate waveguide and TEEY models accuracy," in *2016 IEEE MTT-S International Microwave Symposium (IMS)*, Vol. 23 (IEEE, 2016) pp. 1–4.

[34]J. Cazaux, "Calculated influence of work function on SE escape probability and Secondary Electron Emission yield," Applied Surface Science **257**, 1002–1009 (2010).

[35]G. F. Dionne, "Origin of secondary-electron-emission yield-curve parameters," Journal of Applied Physics **46**, 3347–3351 (1975).

[36]J. R. Young, "Penetration of Electrons and Ions in Aluminum," Journal of Applied Physics **27**, 1–4 (1956).

[37]N. D. Lang and W. Kohn, "Theory of Metal Surfaces: Work Function," Physical Review B **3**, 1215–1223 (1971).

[38]M. Sastry, "On the correlation between the inelastic mean free paths of secondary electrons and the secondary-electron yield parameter in some metal films," Journal of Electron Spectroscopy and Related Phenomena **106**, 93–99 (2000).

[39]K. I. Grais and A. M. Bastawros, "A study of secondary electron emission in insulators and semiconductors," Journal of Applied Physics **53**, 5239–5242 (1982).

[40]C. Weisbuch, H. Benisty, D. Labilloy, R. Houdré, R. P. Stanley, and M. Ilegems, *Confined Electrons and Photons*, edited by E. Burstein and C. Weisbuch, NATO ASI Series, Vol. 340 (Springer US, Boston, MA, 1995) pp. 288–289.

[41]N. Zhang, M. Cao, W.-Z. Cui, and T.-C. Hu, "Effect of rough surface morphology on secondary electron emission from metal surface," Japanese Journal of Applied Physics **56**, 075802 (2017).

[42]V. Baglin, Y. Bozhko, O. Gröbner, B. Henrist, N. Hilleret, C. Scheuerlein, and M. Taborelli, "The Secondary Electron Yield of Technical Material and Its Variation With Surface Treatments," in *EPAC 2000* (Vienna, 2000) pp. 217–221.

[43]A. Plaçais, M. Belhaj, and S. Dadouch, "ONERA copper TEEY measurments with various surface state and incidence angle," Zenodo (2020), 10.5281/zenodo.3648704.

[44]D. Drouin, A. R. Couture, D. Joly, X. Tastet, V. Aimez, and R. Gauvin, "CASINO V2.42—A Fast and Easy-to-use Modeling Tool for Scanning Electron Microscopy and Microanalysis Users," Scanning **29**, 92–101 (2007).

[45]F. Salvat, A. Jablonski, and C. J. Powell, "ELSEPA—Dirac partial-wave calculation of elastic scattering of electrons and positrons by atoms, positive ions and molecules," Computer Physics Communications **165**, 157–190 (2005).

[46]J. R. Lowney, M. T. Postek, Jr., and A. E. Vladar, "Monte Carlo model for SEM linewidth metrology," in *Integrated Circuit Metrology, Inspection, and Process Control VIII*, Vol. 2196, edited by M. H. Bennett (San Jose, CA, 1994) pp. 85–96.

[47]D. C. Joy and S. Luo, "An empirical stopping power relationship for low-energy electrons," Scanning **11**, 176–180 (1989).

[48]G. Wilson and J. R. Dennison, "Approximation of range in materials as a function of incident electron energy," IEEE Transactions on Plasma Science **40**, 291–297 (2012).

[49]C. Inguimbert, J. Pierron, M. Belhaj, and J. Puech, "Extrapolated Range Expression for Electrons Down to 10 eV," in *NSREC* (Portland, USA, 2016).

[50]A. Jablonski, "Elastic backscattering of electrons from surfaces," Surface Science **151**, 166–182 (1985).

[51]R. Oswald, E. Kasper, and K. Gaukler, "A multiple scattering theory of elastic electron backscattering from amorphous surfaces," Journal of Electron Spectroscopy and Related Phenomena **61**, 251–274 (1993).

[52]A. Jablonski, "Angular distribution of elastic electron backscattering from surfaces: determination of the electron inelastic mean free path," Journal of Physics D: Applied Physics **47**, 055301 (2014).